END

MICROCOPY RESOLUTION TEST CHART

NATIONAL BUREAU OF STANDARDS-1963-A

CALCULATION OF IONOSPHERIC PROFILES BY INVERTING VLF/LF REFLECTION DATA: II. Anisotropic Propagation

Pacific Sierra Research Corporation

Chris R. Warber
Edward C. Field, Jr.

APPROVED FOR PUBLIC RELEASE; DISTRIBUTION UNLIMITED

DTIC FILE COPY
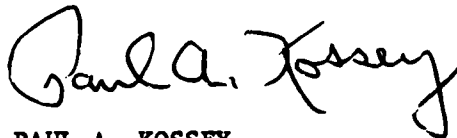
ROME AIR DEVELOPMENT CENTER
Air Force Systems Command
Griffiss Air Force Base, NY 13441-5700

85 01 28 117

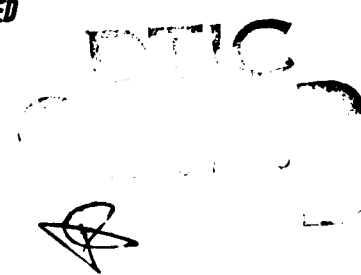This report has been reviewed by the RADC Public Affairs Office (PA) and is releasable to the National Technical Information Service (NTIS). At NTIS it will be releasable to the general public, including foreign nations.

RADC-TR-84-242 has been reviewed and is approved for publication.

APPROVED:

PAUL A. KOSSEY
Project Engineer

APPROVED:

ALLAN C. SCHELL
Chief, Electromagnetic Sciences Division

FOR THE COMMANDER:

JOHN A. RITZ
Acting Chief, Plans Office

If your address has changed or if you wish to be removed from the RADC mailing list, or if the addressee is no longer employed by your organization, please notify RADC (EEPS) Hanscom AFB MA 01731. This will assist us in maintaining a current mailing list.

Do not return copies of this report unless contractual obligations or notices on a specific document requires that it be returned.

REPORT DOCUMENTATION PAGE

1a. REPORT SECURITY CLASSIFICATION	1b. RESTRICTIVE MARKINGS
UNCLASSIFIED	N/A

2a. SECURITY CLASSIFICATION AUTHORITY	3. DISTRIBUTION/AVAILABILITY OF REPORT
N/A	Approved for public release; distribution unlimited
2b. DECLASSIFICATION/DOWNGRADING SCHEDULE	
N/A	

4. PERFORMING ORGANIZATION REPORT NUMBER(S)	5. MONITORING ORGANIZATION REPORT NUMBER(S)
N/A	RADC-TR-84-242

6a. NAME OF PERFORMING ORGANIZATION	6b. OFFICE SYMBOL (If applicable)	7a. NAME OF MONITORING ORGANIZATION
Pacific Sierra Research Corporation		Rome Air Development Center (EEPS)

6c. ADDRESS (City, State and ZIP Code)	7b. ADDRESS (City, State and ZIP Code)
12340 Santa Monica Blvd Los Angeles CA 90025	Hanscom AFB MA 01731

8a. NAME OF FUNDING/SPONSORING ORGANIZATION	8b. OFFICE SYMBOL (If applicable)	9. PROCUREMENT INSTRUMENT IDENTIFICATION NUMBER
Rome Air Development Center	EEPS	F19628-81-C-0083

8c. ADDRESS (City, State and ZIP Code)	10. SOURCE OF FUNDING NOS.			
	PROGRAM ELEMENT NO.	PROJECT NO.	TASK NO.	WORK UNIT NO.
Hanscom AFB MA 01731	61102F	2305	J2	32

11. TITLE (Include Security Classification)
CALCULATION OF IONOSPHERIC PROFILES BY INVERTING VLF/LF REFLECTION DATA: (Cont'd on reverse)

12. PERSONAL AUTHOR(S)
Chris R. Warber, Edward C. Field, Jr.

13a. TYPE OF REPORT	13b. TIME COVERED	14. DATE OF REPORT (Yr., Mo., Day)	15. PAGE COUNT
Final	FROM Apr80 TO Jan84	December 1984	60

16. SUPPLEMENTARY NOTATION
N/A

17. COSATI CODES			18. SUBJECT TERMS (Continue on reverse if necessary and identify by block number)
FIELD	GROUP	SUB. GR.	Ionosounding, Lower Ionosphere,
20	14		VLF/LF Reflection,
			VLF/LF Inverse Problem

19. ABSTRACT (Continue on reverse if necessary and identify by block number)

This report describes a method for inverting VLF/LF reflection data to obtain ionospheric electron densities for conditions in which the geomagnetic field causes the propagation to be anisotropic. It extends an earlier inversion method that was useful only for conditions in which the propagation could be assumed isotropic. The anisotropic method is demonstrated by inverting computer-generated reflection and conversion coefficients for three model ionospheres: SPE-disturbed, ambient daytime, and ambient nighttime. Satisfactory results were obtained for all three cases.

20. DISTRIBUTION/AVAILABILITY OF ABSTRACT	21. ABSTRACT SECURITY CLASSIFICATION
UNCLASSIFIED/UNLIMITED ☒ SAME AS RPT. ☐ DTIC USERS ☐	UNCLASSIFIED

22a. NAME OF RESPONSIBLE INDIVIDUAL	22b. TELEPHONE NUMBER (Include Area Code)	22c. OFFICE SYMBOL
Paul A. Kossey	(617) 861-4265	RADC (EEPS)

DD FORM 1473, 83 APR — EDITION OF 1 JAN 73 IS OBSOLETE.

PREFACE

This report describes a method for inverting VLF/LF reflection data to obtain ionospheric electron densities for conditions in which the geomagnetic field causes the propagation to be anisotropic. It extends an earlier inversion method, also developed for Rome Air Development Center, that was useful only for conditions in which the propagation could be assumed isotropic. The isotropic inversion method was detailed in a companion report: R. E. Warren, E. C. Field, Jr., and C. R. Warber, *Calculation of Ionospheric Conductivity Profiles by Inverting VLF/LF Reflection Data: I. Isotropic Propagation*, Rome Air Development Center, RADC-TR-81-286, October 1981 (also PSR Report 1114, May 1981).

SUMMARY

This report develops an "anisotropic" method for inverting iono-sounder data to calculate ionospheric profiles. It uses conversion coefficients as well as reflection coefficients and, therefore, extends an earlier "isotropic" inversion method that neglected the geomagnetic field and was restricted to disturbed conditions where collisional effects dominate.

The anisotropic and isotropic inversion methods differ primarily in the calculation of Fréchet kernels, which become extremely compli-cated when the geomagnetic field is included. That complexity greatly increases the computer running time needed to obtain numerical solu-tions, and large computers are therefore needed for routine applica-tion. The only other difference is that the anisotropic method finds the electron density profile, whereas the isotropic method finds the conductivity profile. When using the anisotropic method, therefore, it is necessary to input an assumed collision frequency profile.

We demonstrate the anisotropic method by inverting computer-generated reflection and conversion coefficients calculated for known electron density profiles. These coefficients serve as artificial data analogous to those that would be available from ionosounders. We ran three test cases: an SPE-disturbed ionosphere, where collisional effects were dominant; an ambient daytime ionosphere, where collisional effects were comparable to geomagnetic effects; and an ambient night-time ionosphere, where geomagnetic effects were dominant. Despite approximations made to accommodate our small computer, we obtained excellent agreement between calculated and known profiles for the SPE-disturbed and ambient nighttime ionospheres, and fair agreement for the ambient daytime ionosphere.

Those results, which should further improve when a larger computer is used, indicate that the inversion works best when either collisional effects or geomagnetic effects are dominant, and is least accurate when they are comparable. The examples show clearly that the aniso-tropic method must be used for undisturbed conditions. However, for

strongly disturbed conditions, it is preferable to neglect the con-
version coefficients and use the reflection coefficients as inputs to
the isotropic method, which, for that situation, gives quite accurate
results with modest computer running time.

CONTENTS

FIGURES

PREVIOUS PAGE
IS BLANK

SYMBOLS

$\hat{A}$ = admittance matrix

c = velocity of electromagnetic waves in free space

C = cos θ

E_x, E_y, E_z = components of electric field vector $\vec{E}$ of wave

H_e = earth's magnetic field

H_x, H_y, H_z = $Z_0(\mathcal{H}_x, \mathcal{H}_y, \mathcal{H}_z)$

$\mathcal{H}_x$, $\mathcal{H}_y$, $\mathcal{H}_z$ = components of magnetic field vector $\vec{\mathcal{H}}$ of wave

$i = \sqrt{-1}$

$k = \omega/c$

ℓ = direction cosine of earth's magnetic field

m = direction cosine of earth's magnetic field

$\hat{M}$ = susceptibility tensor for ionosphere

n = direction cosine of earth's magnetic field

N = electron density

$\hat{R}$ = reflection coefficient matrix

S = sin θ

$U = 1 - iZ$

x = cartesian coordinate (z is measured vertically upward and x horizontally in plane of incidence)

$X = Ne^2/\varepsilon_0 m\omega^2$, where e and m represent electron charge and mass, respectively

y = cartesian coordinate (z is measured vertically upward and x horizontally in plane of incidence)

$Y = \mu_0 eH_e/m\omega$, where e and m represent electron charge and mass, respectively

z = cartesian coordinate (z is measured vertically upward and x horizontally in plane of incidence)

Z = ν/ω

Z_0 = characteristic impedance of free space, $(\mu_0/\epsilon_0)^{1/2}$

α = azimuth of propagation (measured east of north)

δ = magnetic dip angle, $\lambda - \pi/2$

ϵ_0 = electric permittivity of free space

θ = angle between vertical and wave normal of incident wave below ionosphere

λ = angle geomagnetic field makes with vertical (in northern hemisphere, $\pi/2 < \lambda \leq \pi$)

μ_0 = magnetic permittivity of free space

ν = collision frequency of electrons

ω = $2\pi \times$ frequency of waves

I. INTRODUCTION

This report extends previous analyses to include geomagnetic effects in calculations of ionospheric conductivity profiles. Warren, Field, and Warber [1981] developed a method for inverting VLF/LF ionosounder data to produce such profiles for conditions in which geomagnetic effects are slight. Subsequently, Field, Warren, and Warber [1983] applied the method to reflection coefficient data measured by ionosounders during a strong solar proton event (SPE), when propagation could be assumed isotropic. They presented physical criteria for determining the altitudes at which the inversion is reliable and those where it breaks down.

Because it neglects the geomagnetic field, the "isotropic" inversion method is restricted to conditions in which all important reflections occur at lower altitudes—less than 70 km—where collisional effects dominate geomagnetic effects. Because of that restriction, the method is best suited to strongly disturbed conditions, when ionospheric reflection heights are lower than under normal conditions. It gives only marginal accuracy for undisturbed daytime conditions, and is inapplicable to undisturbed nighttime conditions. Specifically, the isotropic inversion is valid only when the ionospheric conversion coefficients are much smaller than the reflection coefficients.[*]

The present report develops an "anisotropic" inversion method that uses conversion coefficients as well as reflection coefficients and, therefore, accommodates the geomagnetic field. We assume the reader to be familiar with the work of Warren, Field, and Warber [1981] and Field, Warren, and Warber [1983] and do not repeat definitions, derivations, or source citations given by them. The first of those analyses is Vol. I of the present report.

The anisotropic and isotropic inversion methods are conceptually identical. They differ primarily in the calculation of Fréchet kernels,

---

[*]These coefficients are often called converted and normal reflection coefficients, respectively, in the literature.

which become extremely complicated when the geomagnetic field is included. That complexity greatly increases the computer running time needed to obtain numerical solutions, and large computers are therefore needed for routine application. The only other difference is that the anisotropic method finds the electron density profile, whereas the isotropic method finds the conductivity profile. When using the anisotropic method, therefore, it is necessary to input a known collision frequency profile.

Because of the computational complexity of the anisotropic calculations, we demonstrate the method with only three nominal cases. Even for those numerical examples, the limited capacity of Pacific-Sierra Research Corporation's Perkin-Elmer (PE) 3230 computer required us to make certain approximations that would be unnecessary on a larger machine. Also, the examples assume a vertical electric dipole (VED) transmitter and, therefore, omit the reflection and conversion coefficients, $_{\perp}R_{\perp}$ and $_{\perp}R_{\parallel}$, that pertain to the horizontal component of an electric dipole antenna.

We derive the Fréchet kernels in Sec. II and certain other mathematical formulas in the appendixes. Those tedious derivations can be skipped by the reader interested mainly in the method's application. Section III discusses the numerical methods used and tests the anisotropic method by inverting reflection and conversion coefficients calculated for three known profiles. These coefficients serve as artificial data analogous to those that would be available from ionosounders. Section IV summarizes our conclusions.

II. FRÉCHET KERNELS FOR ANISOTROPIC IONOSPHERE

This section finds the anisotropic form of the Fréchet kernels. Once those kernels are known, we treat the reflection coefficient terms $_{\parallel}R_{\parallel}$ and $_{\parallel}R_{\perp}$ as two data points for each frequency and proceed with the inversion as given in Vol. I--except that here we assume the collision frequency to be known and use the inversion to find the electron density profile. Electric and magnetic quantities throughout this report are in mks units.

COORDINATE SYSTEM

Figure 1 shows the electromagnetic wave normal and the earth's magnetic field in the coordinate system used in this report. We assume that the earth is flat, that the wave propagates in the x-direction, and that the wave normal makes an angle θ with the vertical.

SUSCEPTIBILITY MATRIX

To establish our notation, we start with the Maxwell equations for anisotropic media written in matrix form [Budden, 1961]:

$$\frac{d\vec{e}}{dz} = -ik\overleftrightarrow{T}\vec{e} ,$$

where

$$\vec{e} = \begin{pmatrix} E_x \\ -E_y \\ H_x \\ H_y \end{pmatrix}$$
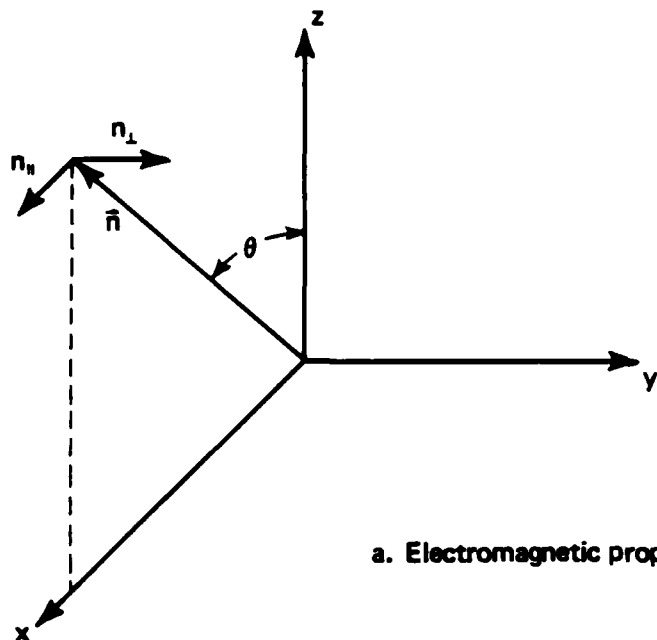
Note: The normal to the wave front lies
in the x-z plane and makes an angle
θ with the vertical: $C = \cos\theta$,
$S = \sin\theta$.
Also, $\vec{n}_{\shortparallel}$ is perpendicular to the wave
normal in the x-z plane, and $\vec{n}_{\perp}$ is
perpendicular to the wave normal
and parallel to the y-axis.

a. Electromagnetic propagation
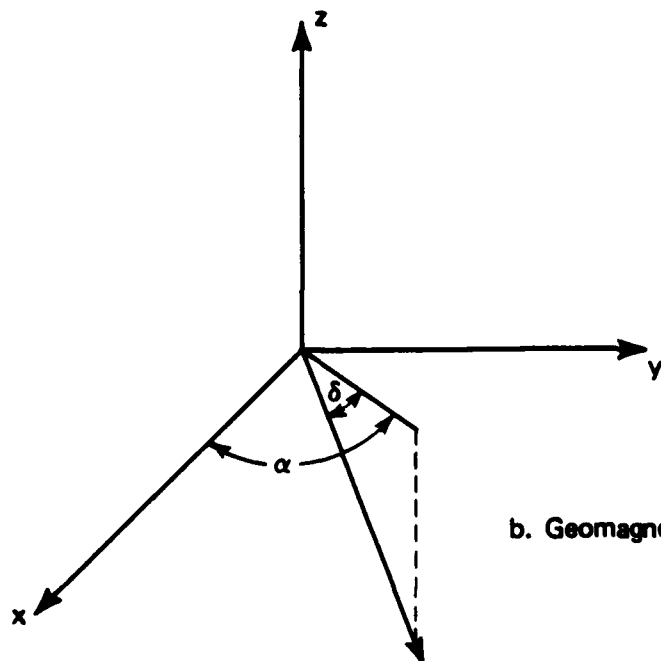
Note: The azimuth of propagation is α
(measured east of magnetic north).
The geomagnetic field makes an
angle of λ with the vertical (in the
northern hemisphere, $90° < \lambda \leq 180°$).
The direction cosines are $\ell = \sin\lambda\cos\alpha$,
$n = \cos\lambda$, $m = \sin\lambda\sin\alpha$.
If we define the dip angle δ so that
$\lambda = \delta + \pi/2$, then $\ell = \cos\delta\cos\alpha$,
$n = -\sin\delta$, $m = \cos\delta\sin\alpha$.

b. Geomagnetic field

Fig. 1--Coordinate system

and

$$
\hat{T} = \begin{pmatrix}
\dfrac{-SM_{31}}{1 + M_{33}} & \dfrac{SM_{32}}{1 + M_{33}} & 0 & \dfrac{C^2 + M_{33}}{1 + M_{33}} \\[2ex]
0 & 0 & 1 & 0 \\[2ex]
\dfrac{M_{23}M_{31}}{1 + M_{33}} - M_{21} & C^2 + M_{22} - \dfrac{M_{23}M_{32}}{1 + M_{33}} & 0 & \dfrac{SM_{23}}{1 + M_{33}} \\[2ex]
1 + M_{11} - \dfrac{M_{13}M_{31}}{1 + M_{33}} & \dfrac{M_{13}M_{32}}{1 + M_{33}} - M_{12} & 0 & \dfrac{-SM_{13}}{1 + M_{33}}
\end{pmatrix} . \tag{1}
$$

Here, the M_{ij} are elements of the susceptibility matrix, which is

$$
\hat{M} = - \frac{X}{U(U^2 - Y^2)} \begin{pmatrix}
U^2 - \ell^2 Y^2 & -inYU - \ell m Y^2 & imYU - \ell n Y^2 \\[2ex]
inYu - \ell m Y^2 & U^2 - m^2 Y^2 & -i\ell YU - mn Y^2 \\[2ex]
-imYU - \ell n Y^2 & i\ell YU - mn Y^2 & U^2 - n^2 Y^2
\end{pmatrix} . \tag{2}
$$

REFLECTION COEFFICIENTS

We can now write the equation for the anisotropic reflection co-efficients, generalized from Budden's equation for admittance:

$$
\frac{2i}{k} \frac{d\hat{R}}{dz} = \hat{S}^{21} + \hat{S}^{22}\hat{R} - \hat{R}\hat{S}^{11} - \hat{R}\hat{S}^{12}\hat{R} , \tag{3}
$$

where the S matrices are given by

$$
\hat{S}^{11} = \begin{pmatrix}
T_{11} + T_{44} + \dfrac{T_{14}}{C} + CT_{41} & -\dfrac{T_{12}}{C} - T_{42} \\[2ex]
-T_{31} - \dfrac{T_{34}}{C} & C + \dfrac{T_{32}}{C}
\end{pmatrix} , \tag{4a}
$$

$$\hat{S}^{12} = \begin{pmatrix} -T_{11} + T_{44} + \dfrac{T_{14}}{C} - CT_{41} & -\dfrac{T_{12}}{C} - T_{42} \\[3mm] T_{31} - \dfrac{T_{34}}{C} & -C + \dfrac{T_{32}}{C} \end{pmatrix}, \qquad (4b)$$

$$\hat{S}^{21} = \begin{pmatrix} -T_{11} + T_{44} - \dfrac{T_{14}}{C} + CT_{41} & \dfrac{T_{12}}{C} - T_{42} \\[3mm] T_{31} + \dfrac{T_{34}}{C} & C - \dfrac{T_{32}}{C} \end{pmatrix}, \qquad (4c)$$

$$\hat{S}^{22} = \begin{pmatrix} T_{11} + T_{44} - \dfrac{T_{14}}{C} - CT_{41} & \dfrac{T_{12}}{C} - T_{42} \\[3mm] -T_{31} + \dfrac{T_{34}}{C} & -C - \dfrac{T_{32}}{C} \end{pmatrix}. \qquad (4d)$$

When we have free space as defined by

$$\frac{X}{U} \ll 1 , \qquad (5)$$

Eq. (3) reduces to a particularly simple form, as follows. Equations (1) and (2) demonstrate that, when Eq. (5) holds, the only important elements of T are

$$T_{14} \cong C^2 , \qquad T_{23} = 1 , \qquad T_{32} \cong C^2 , \qquad T_{41} \cong 1 .$$

Thus, Eqs. (4) reduce to

$$\hat{S}^{11} = 2C\hat{I} , \qquad \hat{S}^{22} = -2C\hat{I} , \qquad \hat{S}^{12} = \hat{S}^{21} = 0 ,$$

yielding, for Eq. (3),

$$\frac{2i}{k} \frac{d\hat{R}}{dz} = -4C\hat{R} \ . \tag{6}$$

The solution of Eq. (6) is

$$R_{ij} = R_{ij}(z_0) \ e^{2Cki(z-z_0)} \ . \tag{7}$$

To calculate R, we start high in the ionosphere where only upgoing waves are present. We integrate Eq. (3) downward until we reach an altitude where Eq. (5) is true. Then we use Eq. (7) for the lower altitudes. Appendix A details the numerical solution of Eq. (3).

DERIVATION OF FRÉCHET KERNELS

The procedure for determining anisotropic Fréchet kernels is parallel to the isotropic procedure of Vol. I, except that we are now dealing with matrices. We let $\hat{R}'$ be the solution of Eq. (3) for electron density $N + \delta N$, and $\hat{R}$ be the solution for electron density N. If we first define $\delta\hat{R}$ by

$$\hat{R}' = \hat{R} + \delta\hat{R} \quad \text{and assume} \quad \hat{S}' = \hat{S} + \frac{\partial\hat{S}}{\partial X} \delta X \ ,$$

where δX is the change in the magnetoionic parameter X, then it can be shown that

$$\frac{2i}{k} \frac{d}{dz} \delta\hat{R} = \hat{S}^{22}\delta\hat{R} - \delta\hat{R}\hat{S}^{11} - \delta\hat{R}\hat{S}^{12}\hat{R} - \hat{R}\hat{S}^{12}\delta\hat{R}$$

$$+ \left(\frac{\partial\hat{S}^{21}}{\partial X} + \frac{\partial\hat{S}^{22}}{\partial X} \hat{R} - \hat{R} \frac{\partial\hat{S}^{11}}{\partial X} - \hat{R} \frac{\partial\hat{S}^{12}}{\partial X} \hat{R} \right) \delta X \ . \tag{8}$$

We can write Eq. (8) in a shorter form as

$$\frac{2i}{k} \frac{d}{dz} \delta\hat{R} = \hat{P}^{(1)}\delta\hat{R} + \delta\hat{R}\hat{P}^{(2)} + \hat{Q}\delta X , \qquad (9)$$

where

$$P_{ij}^{(1)} = S_{ij}^{22} - \sum_k R_{ik}S_{kj}^{12} , \qquad (10a)$$

$$P_{ij}^{(2)} = - S_{ij}^{11} - \sum_k S_{ik}^{12}R_{kj} , \qquad (10b)$$

and

$$Q_{ij} = \frac{\delta S_{ij}^{21}}{\delta X} + \sum_k \frac{\delta S_{ik}^{22}}{\delta X} R_{kj} - \sum_k R_{ik} \frac{\delta S_{kj}^{11}}{\delta X} - \sum_{k\ell} R_{ik} \frac{\delta S_{k\ell}^{12}}{\delta X} R_{\ell j} . \qquad (11)$$

For simplicity, we put Eq. (9) in vector form:

$$\frac{2i}{k} \frac{d}{dz} \begin{pmatrix} \delta R_{11} \\ \delta R_{12} \\ \delta R_{21} \\ \delta R_{22} \end{pmatrix} = \begin{pmatrix} P_{11}^{(1)} + P_{11}^{(2)} & P_{21}^{(2)} & P_{12}^{(1)} & 0 \\ P_{12}^{(2)} & P_{11}^{(1)} + P_{22}^{(2)} & 0 & P_{12}^{(1)} \\ P_{21}^{(1)} & 0 & P_{22}^{(1)} + P_{11}^{(2)} & P_{21}^{(2)} \\ 0 & P_{21}^{(1)} & P_{12}^{(2)} & P_{22}^{(1)} + P_{22}^{(2)} \end{pmatrix}$$

$$\times \begin{pmatrix} \delta R_{11} \\ \delta R_{12} \\ \delta R_{21} \\ \delta R_{22} \end{pmatrix} + \begin{pmatrix} Q_{11} \\ Q_{12} \\ Q_{21} \\ Q_{22} \end{pmatrix} \delta X , \qquad (12)$$

which we can write as

$$\frac{2i}{k} \frac{d}{dz} \delta \mathcal{R} = \mathcal{P} \delta \mathcal{R} + Q \delta X \ . \tag{13}$$

The Fréchet kernel is defined by

$$\delta \mathcal{R}(z) \equiv \int_z^{z_m} G(z, z') \delta X(z') \ dz' \ . \tag{14}$$

Taking the derivative, we get

$$\frac{2i}{k} \frac{d}{dz} \delta \mathcal{R} = \frac{2i}{k} \left[-G(z, z)\delta X(z) + \int_z^{z_m} dz' \ \frac{\partial}{\partial z} G(z, z')\delta X(z') \right] \ . \tag{15}$$

However, we can also combine Eq. (14) with Eq. (13), obtaining

$$\frac{2i}{k} \frac{d}{dz} \delta \mathcal{R} = \mathcal{P}(z) \int_z^{z_m} G(z, z')\delta X(z') \ dz' + Q(z)\delta X(z')$$

$$= \int_z^{z_m} \mathcal{P}(z) G(z, z')\delta X(z') \ dz' + Q(z)\delta X(z) \ . \tag{16}$$

Thus, comparing Eqs. (15) and (16), we see that

$$- \frac{2i}{k} G(z, z) = Q(z) \tag{17}$$

and

$$\frac{2i}{k} \frac{\partial}{\partial z} G(z, z') = \mathcal{P}(z) G(z, z') \ . \tag{18}$$

Since the reflection coefficient data are known at the ground, the Fréchet kernel we need for the inversion is $G(0, z)$. However, the differential equation (18) can be time-consuming to solve for a large number of altitudes. For small coupling between the modes, we can use the following self-consistent method. Equations (17) and (18) and the definition of $\mathscr{P}$ in Eq. (12) yield

$$G_1(z, z') = -\frac{k}{2i} \exp\left[-\frac{k}{2i} \int_z^{z'} dz'' \, \mathscr{P}_{11}(z'')\right] \left\{ Q_1(z') \right.$$

$$+ \int_z^{z'} dz'' \left[\mathscr{P}_{12}(z'') G_2(z'', z') + \mathscr{P}_{13}(z'') G_3(z'', z')\right]$$

$$\left. \times \exp\left[\frac{k}{2i} \int_{z''}^{z'} \mathscr{P}_{11}(z''') \, dz'''\right]\right\}, \tag{19a}$$

$$G_2(z, z') = -\frac{k}{2i} \exp\left[-\frac{k}{2i} \int_z^{z'} dz'' \, \mathscr{P}_{22}(z'')\right] \left\{ Q_2(z') \right.$$

$$+ \int_z^{z'} dz'' \left[\mathscr{P}_{21}(z'') G_1(z'', z') + \mathscr{P}_{24}(z'') G_4(z'', z')\right]$$

$$\left. \times \exp\left[\frac{k}{2i} \int_{z''}^{z'} \mathscr{P}_{22}(z''') \, dz'''\right]\right\}, \tag{19b}$$

$$G_3(z, z') = -\frac{k}{2i} \exp\left[-\frac{k}{2i} \int_z^{z'} dz'' \; \mathscr{P}_{33}(z'')\right]\left\{Q_2(z')\right.$$

$$+ \int_z^{z'} dz'' \left[\mathscr{P}_{31}(z'') \, G_1(z'', z') + \mathscr{P}_{34}(z'') \, G_4(z'', z')\right]$$

$$\left. \times \exp\left[\frac{k}{2i} \int_{z''}^{z'} \mathscr{P}_{33}(z''') \; dz'''\right]\right\}, \tag{19c}$$

$$G_4(z, z') = -\frac{k}{2i} \exp\left[-\frac{k}{2i} \int_z^{z'} dz'' \; \mathscr{P}_{44}(z'')\right]\left\{Q_4(z')\right.$$

$$+ \int_z^{z'} dz'' \left[\mathscr{P}_{42}(z'') \, G_2(z'', z') + \mathscr{P}_{43}(z'') \, G_3(z'', z')\right]$$

$$\left. \times \exp\left[\frac{k}{2i} \int_{z''}^{z'} \mathscr{P}_{44}(z''') \; dz'''\right]\right\}. \tag{19d}$$

We first solve Eqs. (19a) and (19d) assuming that G_2 and G_3 are zero. Then, to calculate G_2 and G_3, we substitute the results into Eqs. (19b) and (19c). Those results are in turn reapplied to Eqs. (19a) and (19d), and G_1, G_4 are recalculated. The process is repeated until G_1, G_2, G_3, G_4 stop changing.

Computation time can be saved if we use the solution of the Fréchet kernel in the free space between the earth and the ionosphere. Recall that, starting from Eq. (5), we found that

$$S^{11} = 2C \begin{pmatrix} 1 & 0 \\ 0 & 1 \end{pmatrix}, \qquad S^{22} = -2C \begin{pmatrix} 1 & 0 \\ 0 & 1 \end{pmatrix}, \qquad S^{12} = S^{21} = 0 .$$

Therefore, Eqs. (10) yield

$$P^{(1)}_{ij} = -2C\delta_{ij} \quad \text{and} \quad P^{(2)}_{ij} = -2C\delta_{ij} ,$$

and so from Eq. (12) we obtain

$$\mathcal{P}_{ij} = -4C\delta_{ij} . \tag{20}$$

Thus, Eqs. (19) can be written as

$$G_i(z, z') = -\frac{k}{2i} e^{+2ikC(z'-z)} Q_i(z') . \tag{21}$$

Now the solutions we need are $G_i(0, z)$, so

$$G_i(0, z') = -\frac{k}{2i} e^{2ikCz'} Q_i(z') \tag{22}$$

as long as $z' < z_{BOT}$, where z_{BOT} is the bottom of the ionosphere. Assume $z' > z_{BOT}$. Then

$$G_i(0, z') = -\frac{k}{2i} \exp\left[-\frac{k}{2i} \int_0^{z'} dz'' \, \mathcal{P}_{ii}(z'') \right] \left\{ Q_i(z') + \int_0^{z'} dz'' \right.$$

$$\times \left[\sum_{\substack{k \\ k \neq i}} \mathcal{P}_{ik} G_k(z'', z') \right] \exp\left[\frac{k}{2i} \int_{z''}^{z'} \mathcal{P}_{ii}(z''') \, dz''' \right] \right\} .$$

$$\tag{23}$$

Since

$$\int_0^{z'} = \int_0^{z_{BOT}} + \int_{z_{BOT}}^{z'}$$

and

$$\mathcal{P}_{ik} = 0 \quad \text{for} \quad z < z_{BOT} \;,$$

we obtain for Eq. (23)

$$G_i(0, z') = e^{2ikCz_{BOT}} \left[-\frac{k}{2i} \exp\left[-\frac{k}{2i} \int_{z_{BOT}}^{z'} dz'' \, \mathcal{P}_{ii}(z'') \right] \left\{ Q_i(z') \right. \right.$$

$$\left. \left. + \int_{z_{BOT}}^{z'} dz'' \sum_{\substack{k \\ k \neq i}} \mathcal{P}_{ik} \, G_k(z'', z') \, \exp\left[\frac{k}{2i} \int_{z''}^{z'} \mathcal{P}_{ii}(z''') \, dz''' \right] \right\} \right]$$

$$= e^{2ikCz_{BOT}} \, G_i(z_{BOT}, z') \;. \tag{24}$$

Thus, we must solve Eqs. (19) only within the ionosphere. Elsewhere, we can use Eqs. (22) and (24).

III. TEST CASES USING KNOWN PROFILES

The three nominal cases presented here apply the anisotropic inversion method to conditions under which geomagnetic effects are, respectively, slight, moderate, and strong. We assume a VED transmitting antenna and therefore require only reflection coefficients $_{\|}R_{\|}$ and conversion coefficients $_{\|}R_{\perp}$ to perform the inversion. However, $_{\perp}R_{\perp}$ and $_{\perp}R_{\|}$ can easily be incorporated to accommodate the horizontal component of nonvertical antennas.

When geomagnetic effects are important, the particle densities and collision frequencies appear explicitly in the Fréchet kernels and admittance matrix. We have assumed the collision frequencies to be known (see Appendix B) and solved for electron density profiles. This procedure is different from that used in the isotropic inversion of Vol. I, where the assumed absence of the geomagnetic field permitted the Fréchet kernels and wave admittance to be expressed solely in terms of the scalar conductivity, which was calculated directly.

We begin the inverse solution of the example cases by calculating $_{\|}R_{\|}$ and $_{\|}R_{\perp}$ for the three electron density profiles assumed, and hereafter referred to as "true." These coefficients serve as artificial data analogous to those that would be available from ionosounders. All calculations were done for an azimuth of -90 deg, a geomagnetic dip angle of 60 deg, and a geomagnetic field strength of 0.54 G. Those parameters represent mid-latitude east-west propagation in the northern hemisphere. We further assume an incidence angle of 60 deg.

COMPUTATIONAL DIFFICULTIES

The computer code that we developed for the anisotropic inversion is too large to be easily run on the PE 3230. However, it should be within the capacity of the large computers that are commonly available at government facilities and that will be used for routine applications of the anisotropic inversion. Therefore, the size of the code should present no problem in the future. Nonetheless, it was convenient to run our test cases on the PE 3230 and, to do so, we had to make two

approximations to reduce computer running time. We emphasize that those approximations, discussed below, will probably be unnecessary when the code is run on a large computer. Moreover, since the PE 3230 uses only 32-bit words, we believe that round-off errors occurred. We expect greater accuracy when the code is run on a 64-bit machine.

The computer implementation of the anisotropic inversion is straightforward--essentially the same as described in Vol. I--except that the calculation of the Fréchet kernels is extremely time-consuming. Even using the self-consistent calculation described in Sec. II, we found the execution time on the PE 3230 to be about 1 CPU-minute per frequency per iteration. A typical anisotropic inversion requires about 5 frequencies and 30 iterations and, therefore, about 150 CPU-minutes. Such execution times are impractical, so we made two approximations.

Our first approximation was to double the spacing between the altitudes at which the kernels are calculated, and then interpolate to find the kernels at the intermediate altitudes. Second, and of greater consequence, we assume the kernels to quickly fall to zero at altitudes above those where the self-consistent approximation is valid. Such an approach avoids exhaustive calculation of the kernels at altitudes too high to have much effect on the ground-level reflection coefficients. Numerical checks indicate that the inversion depends only slightly on the value of the kernels at such high altitudes. That fact, coupled with the satisfactory agreement between true and calculated profiles found for the examples discussed below, indicates that both approximations are good, although probably unnecessary for a large computer. Their practical effect is a fourfold reduction in computation time.

EXPONENTIAL FIT TO SPE-DISTURBED PROFILE

For our first example, we assume an exponential electron density profile given by

$$N_e(z) = 2 \times 10^9 \, e^{(z-45)/4} \quad e/m^3 \, . \tag{25}$$

When combined with the electron collision frequency profile in Appendix B, Eq. (25) produces an exponential conductivity profile that approximates the polar ionosphere between about 40 and 50 km at 1508 UT on 4 August 1972, the peak period of a strong SPE[*] [Reagan et al., 1982]. That conductivity profile was used in Vol. I as an example for testing the isotropic inversion method.

Table 1 lists the reflection and conversion coefficients calculated for the profile given by Eq. (25). As expected for a strong SPE, the conversion coefficients are much smaller than the reflection coefficients. The anisotropic inversion should therefore produce nearly the same results as the isotropic inversion.

Table 1

REFLECTION AND CONVERSION COEFFICIENTS CALCULATED
FOR MODEL OF SPE-DISTURBED IONOSPHERE, EQ. (25)

Frequency (kHz)	Reflection Coefficient, $\|_\| R_\|\|$	Conversion Coefficient, $\|_\| R_\perp\|$	$\|_\| R_\perp\| / \|_\| R_\|\|$
5	0.341	0.009	0.027
7	0.307	0.009	0.030
10	0.267	0.009	0.034
18	0.167	0.007	0.040
30	0.069	0.003	0.048

Figure 2 shows the agreement between the true profile and that calculated using the anisotropic inversion. As expected, these results correspond well to those reported in Vol. I for the isotropic inversion. Specifically, we find close agreement between the true and calculated

_____

[*]The electron density profile in Eq. (25) is physically unrealistic in two respects. First, an SPE would not disturb the ionosphere at the mid-latitude assumed here. Second, ions rather than electrons dominate the conductivity below, say, 50 km, so Eq. (25) is actually an "effective" electron density. Nonetheless, the profile is suitable for our present purpose--namely, verifying the mathematical accuracy of the anisotropic inversion.
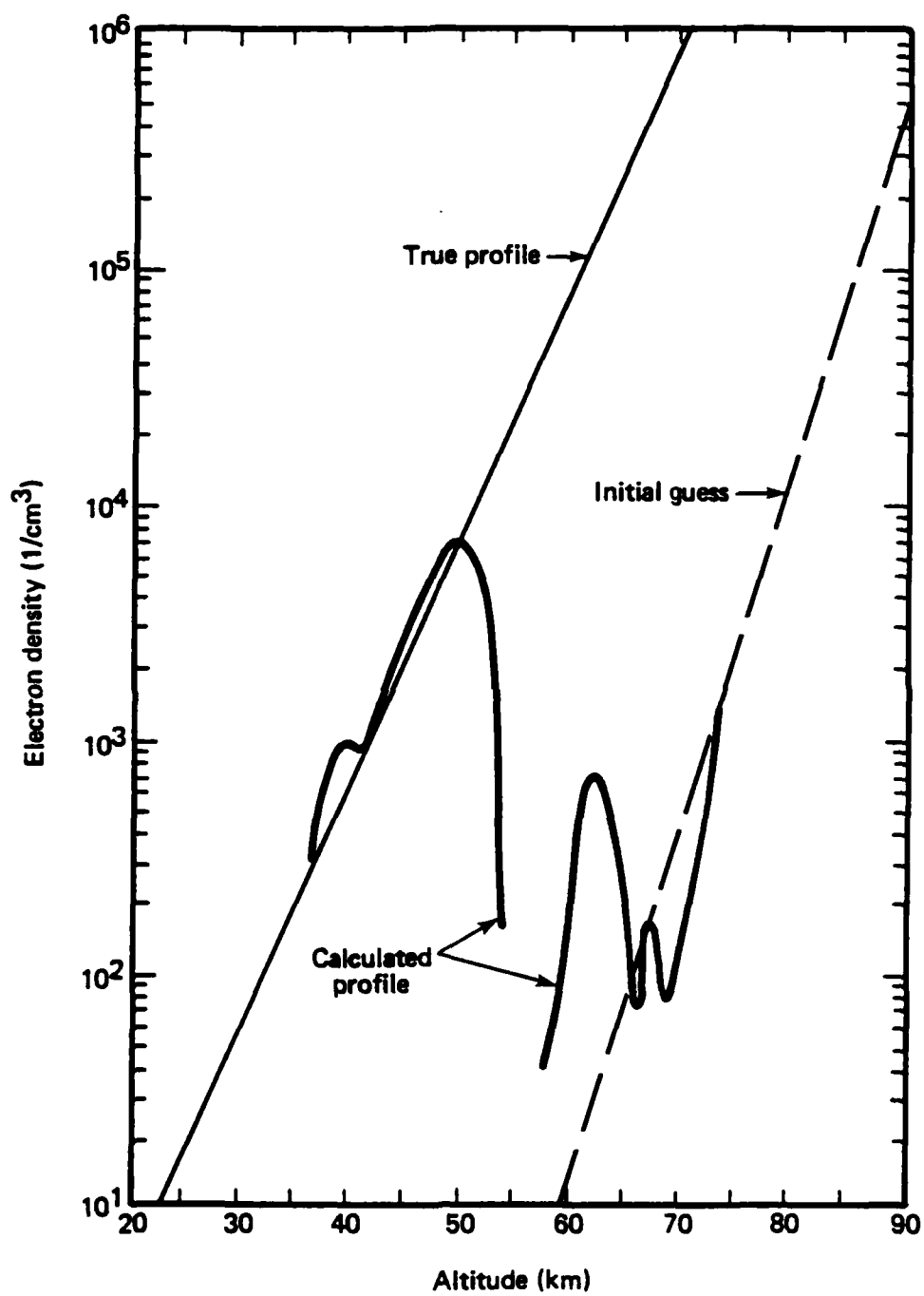
Fig. 2--Calculated and true profiles for SPE-disturbed iono-
sphere--Eq. (25) and anisotropic inversion

profiles at altitudes from about 40 to 50 km, and poorer agreement outside that range.

In Vol. I and the subsequent paper by Field, Warren, and Warber [1983], we identified physical criteria for determining the altitudes at which VLF/LF reflection data yield reliable profiles. The most useful of those criteria was based on calculation of an upgoing wave, $\widetilde{H}$, normalized to unity at the ground. The calculated profiles were most reliable at altitudes where $0.5 \lesssim \widetilde{H} < 1$, because the ionosphere at those altitudes most strongly affects the ground-level reflection coefficients. At low altitudes, where $\widetilde{H} \approx 1$, the ionosphere is too rarefied to cause substantial reflection. At high altitudes, where $\widetilde{H} \leq 0.5$, the signal is too weak and the return too weak, even if the reflectivity is high.

Inclusion of the geomagnetic field precludes derivation of a simple quantity like $\widetilde{H}$. Therefore, we derive in Appendix C two complicated quantities, U_{11} and U_{21}, that combine upgoing electric and magnetic fields and can be used to assess the range of validity of the anisotropic inversion—much as $\widetilde{H}$ was used to assess the range of validity of the isotropic inversion. The quantities U_{11} and U_{21} are normalized to 1 and 0 at the ground, respectively. However, U_{11} does not become $\widetilde{H}$ if the geomagnetic field vanishes, nor is the application of U_{11} and U_{21} for the anisotropic inversion so unequivocal as the application of $\widetilde{H}$ for the isotropic inversion. One difficulty is that the differential equations for U_{11} have a mathematical property known as *stiffness*, which causes numerical inaccuracies—but, fortunately, only at high altitudes that exceed those where the most important reflections occur. We use U_{11} and U_{21} in all three nominal cases examined in this report.

Figures 3 and 4 plot U_{11} and U_{21} for the calculated profile shown in Fig. 2 and, respectively, frequencies of 5 and 30 kHz. For both frequencies, the condition $0.5 \lesssim U_{11} < 1$ is satisfied in the altitude range for which the calculated and true profiles agree, and is not satisfied for higher or lower altitudes. Therefore, this example confirms that U_{11} provides a means of assessing the range of validity of an inversion based on ionosounder data for which no true profile is available for comparison.
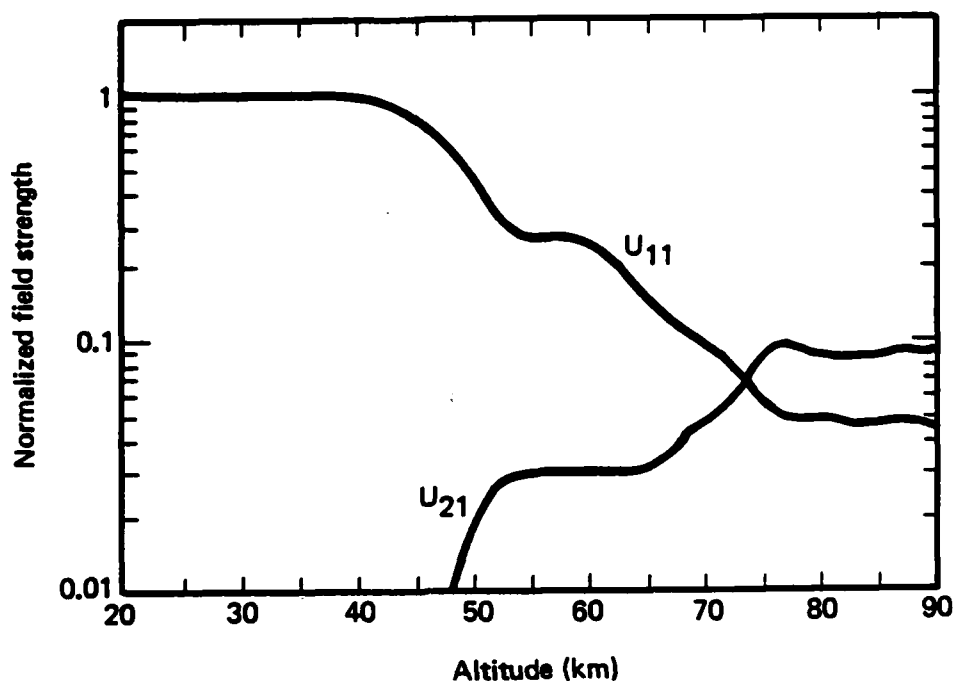
Fig. 3--Normalized field strength versus altitude for
calculated profile of Fig. 2 and 5 kHz

Field, Warren, and Warber [1983] used the isotropic inversion
method to calculate conductivity profiles from ionosounder data mea-
sured during a strong SPE. That method uses only $_{||}R_{||}$ data as inputs,
so $_{||}R_\perp$ data must be ignored. The error incurred by that procedure
could not be determined, but it was argued that great accuracy should
be expected because $_{||}R_\perp \ll {}_{||}R_{||}$ at all frequencies used.

We can now evaluate the accuracy of the above procedure by using
values of $_{||}R_{||}$ from Table 1 as inputs to the isotropic inversion method
and ignoring $_{||}R_\perp$. The results, shown in Fig. 5, are reassuring. In
fact, the agreement between the calculated and true profiles is slightly
better in Fig. 5 than for the anisotropic inversion plotted in Fig. 2.
That apparently puzzling result is easily explained. The slight in-
crease in accuracy gained by retaining $_{||}R_\perp$ is more than offset by the
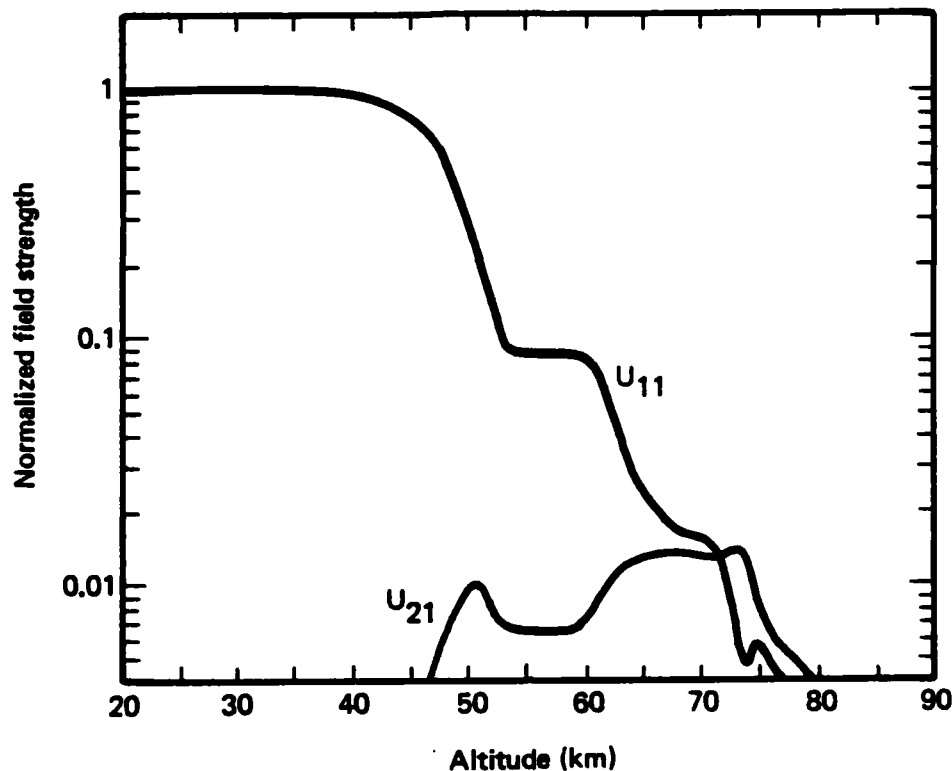
Fig. 4--Normalized field strength versus altitude for
calculated profile of Fig. 2 and 30 kHz

loss of numerical accuracy incurred by using the more detailed aniso-
tropic method.[*] Because for this example the anisotropic inversion
requires much longer computer time without giving more accurate re-
sults, we conclude that *the isotropic method should always be used if*
$_{||}R_{\perp} \ll {}_{||}R_{||}$ *at all frequencies for which data are available.*

_____

[*]This conclusion applies to results calculated on the PE 3230
and could be different for calculations on larger computers, for which
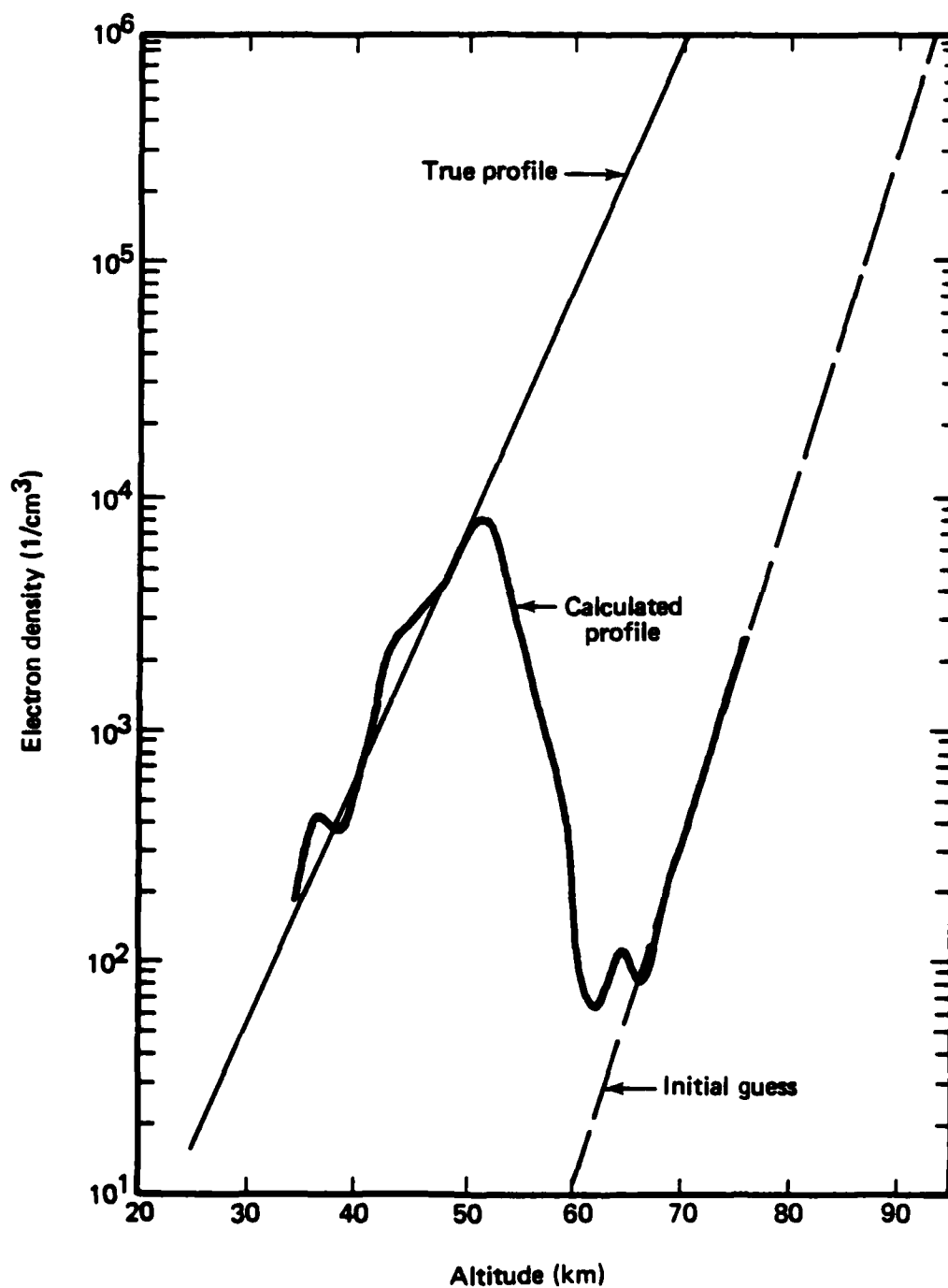round-off errors are smaller and approximations are not required.

Fig. 5--Calculated and true profiles for SPE-disturbed ionosphere--
Eq. (25) and isotropic inversion, using $_{\|}R_{\|}$ as input

EXPONENTIAL FIT TO AMBIENT DAYTIME PROFILE

Our second example assumes an exponential electron density profile given by

$$N_e(z) = 4 \times 10^8 \, e^{0.35(z-70)} \quad e/m^3 , \qquad (26)$$

which approximates ambient daytime conditions. The calculated reflection and conversion coefficients are shown in Table 2. Since the conversion coefficients are of the same order of magnitude as the reflection coefficients, geomagnetic effects should be important. The large ratio of $_{\|}R_{\perp}$ to $_{\|}R_{\|}$ at the higher frequencies is caused by $_{\|}R_{\|}$ being small rather than $_{\|}R_{\perp}$ being large. That effect, which could be due to a quasi-Brewster's angle, could cause the geomagnetic effect at the chosen parameter values (for incidence angle, azimuth) to be greater than for other daytime conditions. The computational limitations of the PE 3230 preclude calculating several cases to test that possibility.

Table 2

REFLECTION AND CONVERSION COEFFICIENTS CALCULATED FOR
MODEL OF AMBIENT DAYTIME IONOSPHERE, EQ. (26)

Frequency (kHz)	Reflection Coefficient, $\|_{\|}R_{\|}\|$	Conversion Coefficient, $\|_{\|}R_{\perp}\|$	$\|_{\|}R_{\perp}\| / \|_{\|}R_{\|}\|$
5	0.277	0.181	0.654
7	0.233	0.200	0.858
10	0.194	0.211	1.090
18	0.133	0.194	1.459
30	0.092	0.132	1.430

The numerical results for ambient daytime conditions, shown in Figs. 6 through 9, follow the same sequence as those of Figs. 2 through 5. Figure 6 shows that the anisotropic inversion gives good results at altitudes between about 64 and 70 km, and poor results outside that range. Overall, however, the anisotropic results are poorer than those
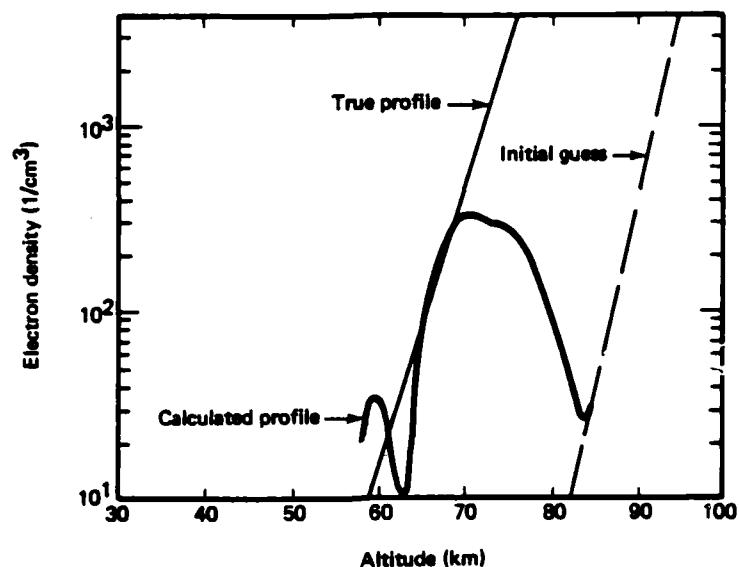
Fig. 6--Calculated and true profiles for ambient daytime
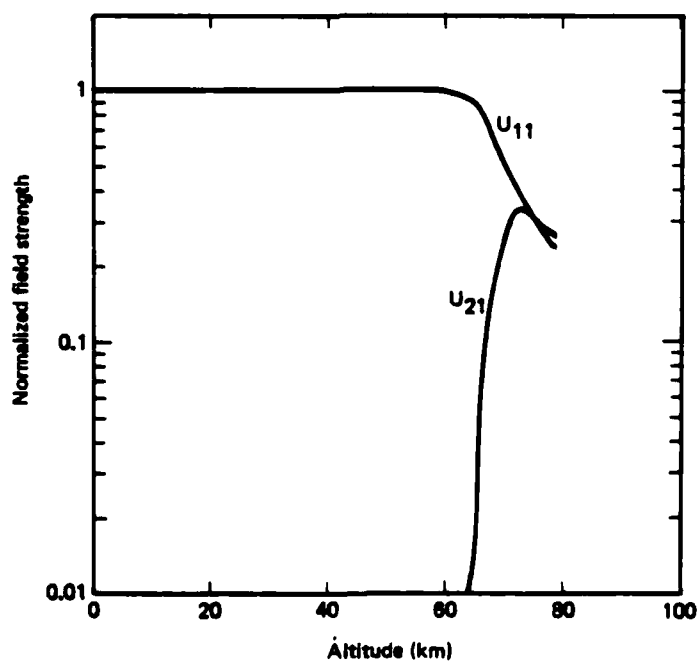ionosphere--Eq. (26) and anisotropic inversion

Fig. 7--Normalized field strength versus altitude for
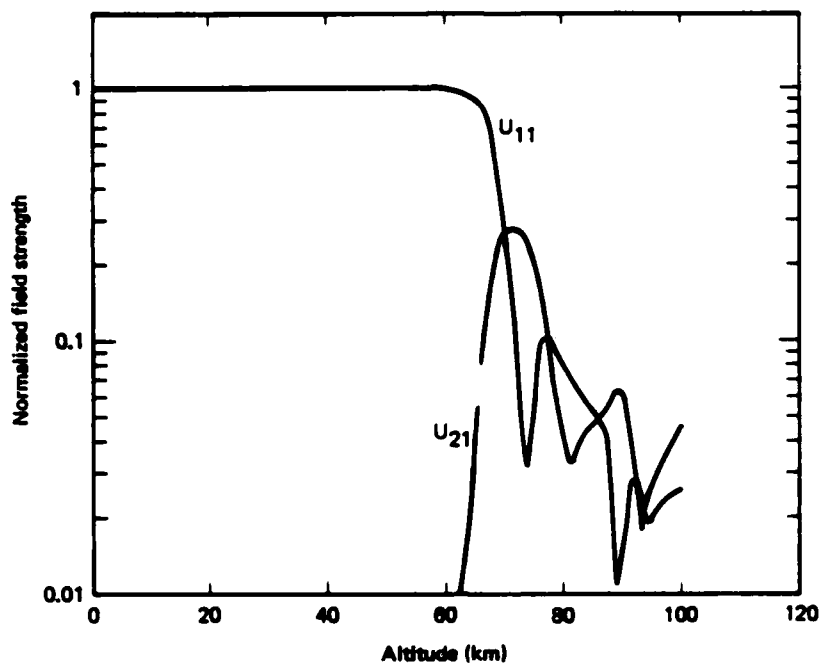calculated profile of Fig. 6 and 5 kHz

Fig. 8--Normalized field strength versus altitude for
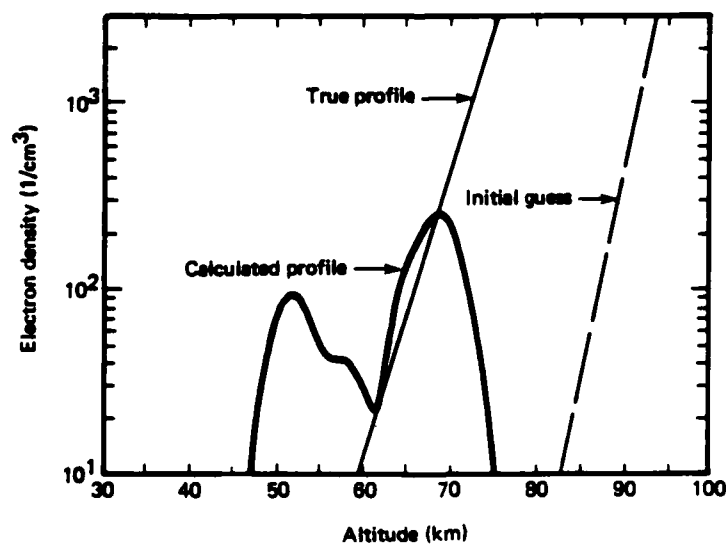calculated profile of Fig. 6 and 30 kHz

Fig. 9--Calculated and true profiles for ambient daytime
ionosphere--Eq. (26) and isotropic inversion,
using $_{||}R_{||}$ as input

obtained with the isotropic method and presented by Field, Warren, and Warber [1983], which showed close agreement between calculated and true values in the 60 to 70 km range for a nominal daytime profile. The degradation in accuracy is almost certainly caused by computational errors associated with the complicated anisotropic equations, but re-calculation on a larger computer is needed to verify that explanation.

Figures 7 and 8 show the normalized upgoing fields U_{11} and U_{21}. As in the previous example, the altitude range defined by the condition $0.5 \le U_{11} < 1$--roughly 60 to 70 km--corresponds to the 64 to 70 km range where the anisotropic inversion works best.

Recall that the better agreement obtained by Field, Warren, and Warber [1983] with the isotropic method was based on artificial data generated by neglecting the geomagnetic field, and does *not* imply that the isotropic inversion should be used instead of the anisotropic in-version for reflection coefficients actually measured during the day-time. Figure 9 confirms the somewhat poorer accuracy that would be achieved by using the isotropic method to invert measured reflection coefficients. Specifically, we ignore the values of $_{\parallel}R_{\perp}$ shown in Table 2 and use only values of $_{\parallel}R_{\parallel}$. As expected, the agreement between the calculated and true profiles is not quite as good as that shown in Fig. 6 for the anisotropic inversion.

AMBIENT NIGHTTIME PROFILE

We used the profile given by Pappert and Moler [1974], labeled true profile in Fig. 10, to test the anisotropic inversion under am-bient nighttime conditions. The reflection and conversion coefficients calculated for that profile are given in Table 3. Since $_{\parallel}R_{\perp}$ is large, geomagnetic effects would be expected to dominate collisional effects. Figure 10 shows that the calculated and true profiles agree very well at altitudes between 73 and 85 km. In fact, the overall agreement is much better than that achieved for the ambient daytime model and indi-cates that the anisotropic inversion works best--on the PE 3230 com-puter, at least--when geomagnetic effects are dominant.
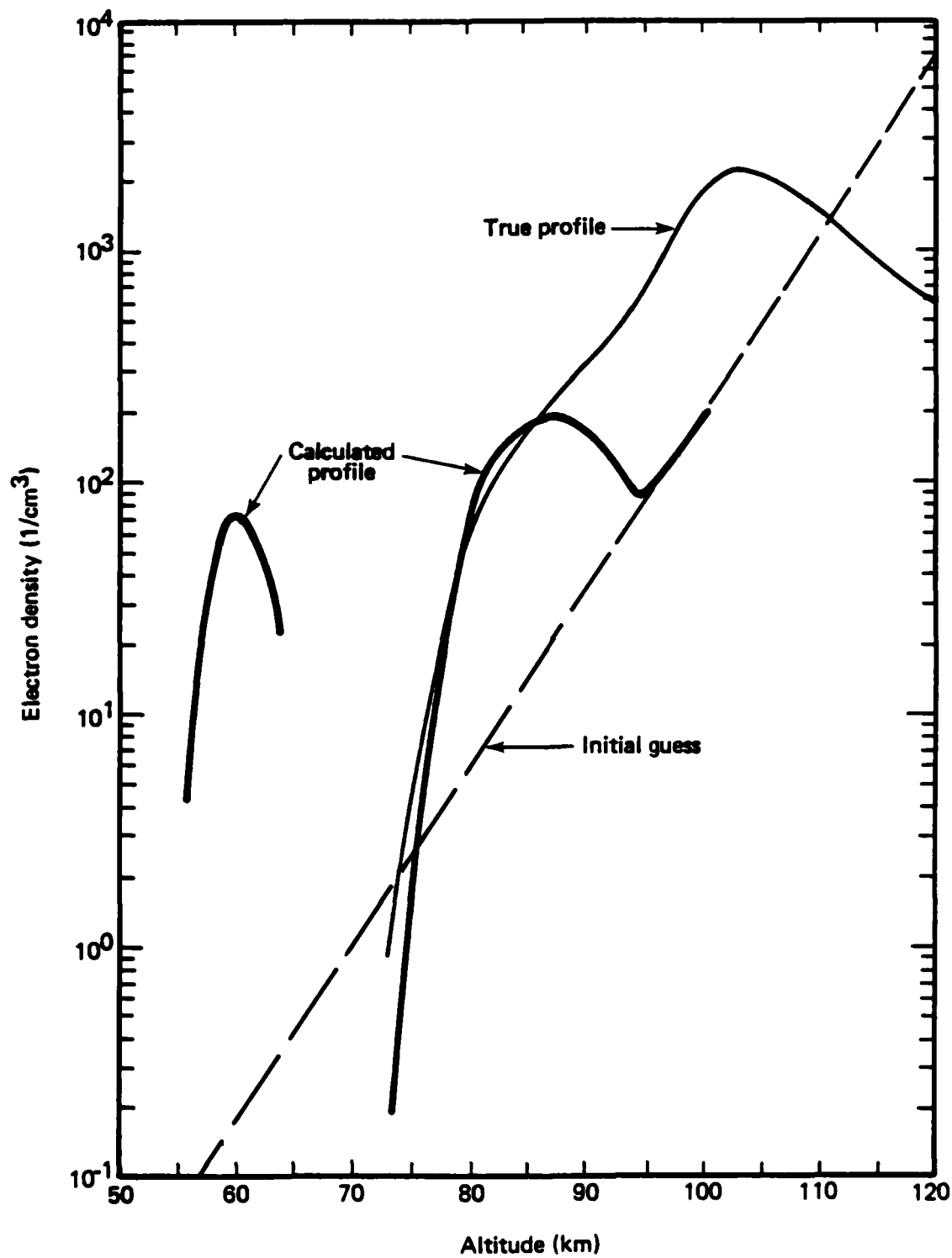
Fig. 10--Calculated and true profiles for ambient nighttime
ionosphere--anisotropic inversion

Table 3

REFLECTION AND CONVERSION COEFFICIENTS CALCULATED FOR
MODEL OF AMBIENT NIGHTTIME IONOSPHERE, FIG. 10

Frequency (kHz)	Reflection Coefficient, $\|_{||}R_{||}\|$	Conversion Coefficient, $\|_{||}R_{\perp}\|$	$\|_{||}R_{\perp}\|/\|_{||}R_{||}\|$
5	0.322	0.392	1.218
7	0.267	0.467	1.746
10	0.251	0.504	2.011
18	0.335	0.418	1.250
30	0.275	0.318	1.159

Figures 11 and 12 show that the condition $0.5 \lesssim U_{11} < 1$ works well to define the height range over which the anisotropic inversion is most reliable. Further, the behavior of U_{11} indicates the spuriousness of the layer shown by Fig. 10 to occur at around 60 km. That layer affects the fields only slightly, because collisional effects cause electrons at 60 km altitude to be much less mobile than electrons at 73 to 85 km. Its artificiality is confirmed by Figs. 11 and 12, which show that U_{11} changes only slightly in the vicinity of the spurious layer. It is, of course, possible that the layer would not appear if the inversions had been performed on a larger computer.

Figure 13 shows the consequences of ignoring $_{||}R_{\perp}$ and using only $_{||}R_{||}$ in the isotropic inversion method. Such a procedure is equivalent to using the isotropic inversion method in conjunction with ionosounder data measured at night. As expected, the calculated and true profiles totally disagree. Of course, the anisotropic method must be used for ambient nighttime conditions.
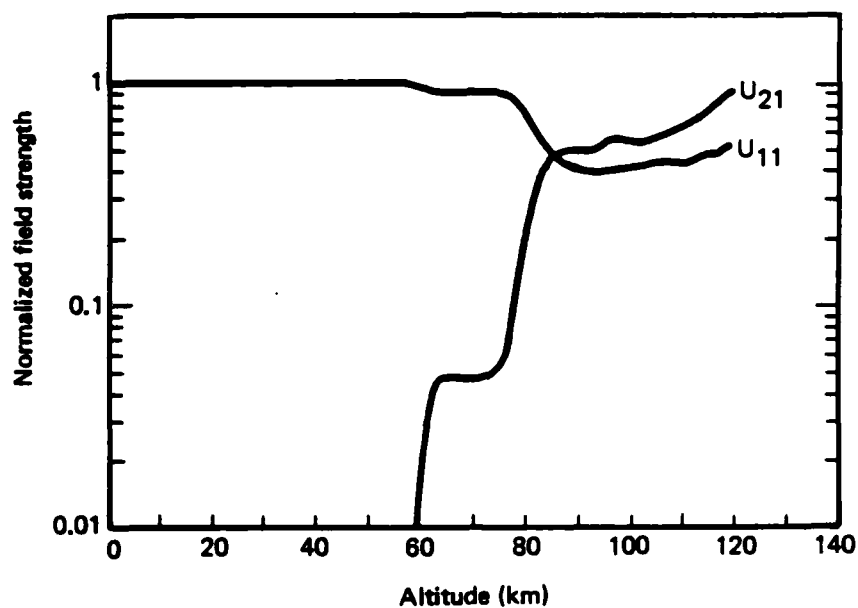
Fig. 11--Normalized field strength versus altitude for
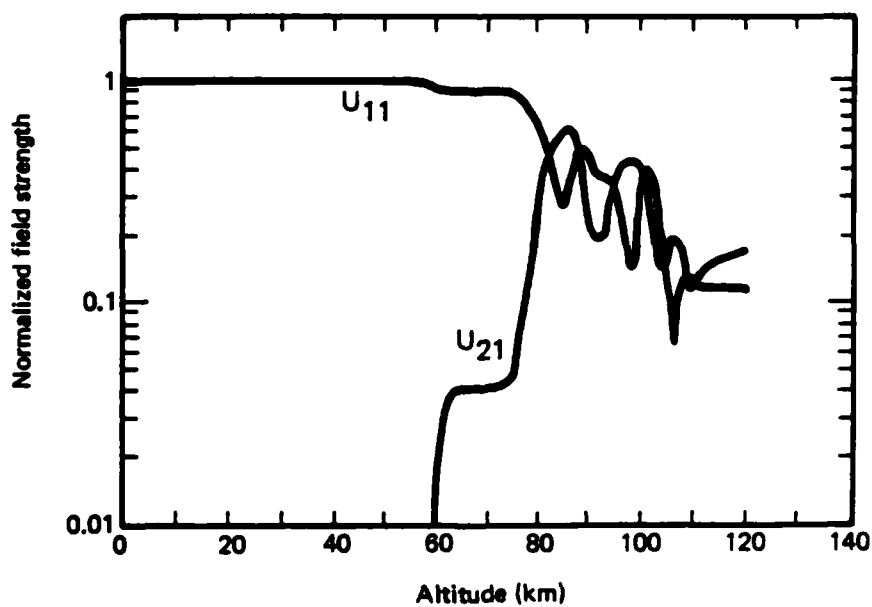calculated profile of Fig. 10 and 5 kHz

Fig. 12--Normalized field strength versus altitude for
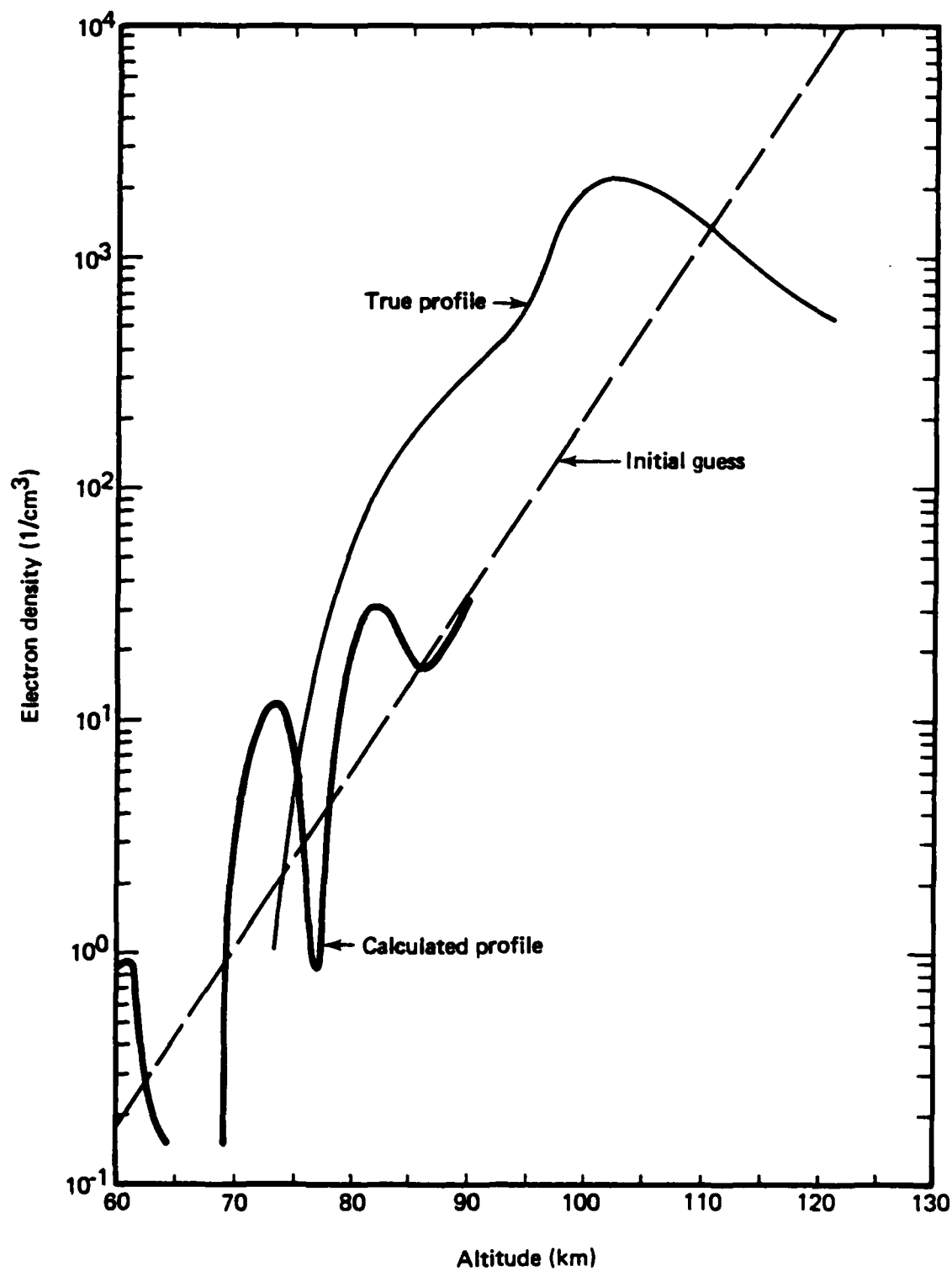calculated profile of Fig. 10 and 30 kHz

Fig. 13--Calculated and true profiles for ambient nighttime
ionosphere--isotropic inversion, using $_{||}R_{||}$ as input

IV. CONCLUSIONS

We tested the anisotropic inversion method for three cases: an SPE-disturbed ionosphere, where collisional effects were dominant; an ambient daytime ionosphere, where collisional effects were comparable to geomagnetic effects; and an ambient nighttime ionosphere, where geomagnetic effects were dominant. Despite approximations made to accommodate our small computer, we obtained excellent accuracy for the SPE-disturbed and ambient nighttime ionospheres, and fair accuracy for the ambient daytime ionosphere.

Those results, which should further improve when a larger computer is used, indicate that the inversion works best when either collisional effects or geomagnetic effects are dominant, and is least accurate when they are comparable. The examples show clearly that the anisotropic method must be used for undisturbed conditions. However, for disturbed conditions, when $_{||}R_{\perp} \ll {}_{||}R_{||}$, it is preferable to neglect $_{||}R_{\perp}$ and use values of $_{||}R_{||}$ as inputs to the isotropic method, which, for that situation, gives quite accurate results with modest computer running time.

Appendix A

CALCULATION OF FORWARD PROBLEM

This appendix presents our method of calculating the forward problem—which determines the reflection coefficients, given the electron density. Strictly, the forward problem is the solution of Eq. (3) in Sec. II. In practice, however, we can save computer time by solving for the admittance rather than the reflection coefficients, and then using [Budden, 1961]

$$\hat{R} = \begin{pmatrix} 1 & 0 \\ \\ 0 & -1 \end{pmatrix} + 2 \begin{pmatrix} -CA_{11} - 1 & A_{12} \\ \\ A_{21} & 1 - \dfrac{A_{22}}{C} \end{pmatrix}^{-1}$$

to find $\hat{R}$. Since we solve only for $\hat{A}$ within the ionosphere, we avoid numerical instabilities.

DEFINITION OF ADMITTANCE

We start with Budden's equation for admittance [Budden, 1961]:

$$\frac{i}{k} \frac{\partial \hat{A}}{\partial z} = \hat{\tau}_{21} + \hat{A}\hat{\tau}_{11} + \hat{\tau}_{22}\hat{A} + \hat{A}\hat{\tau}_{12}\hat{A} \;, \tag{A.1}$$

where

$$\hat{\tau}_{11} = \begin{pmatrix} -T_{11} & T_{12} \\ \\ 0 & 0 \end{pmatrix}, \tag{A.2a}$$

$$\hat{\tau}_{12} = \begin{pmatrix} -T_{14} & 0 \\ \\ 0 & 1 \end{pmatrix}, \tag{A.2b}$$

$$\hat{\tau}_{21} = \begin{pmatrix} T_{41} & -T_{42} \\ T_{31} & -T_{32} \end{pmatrix} , \qquad (A.2c)$$

$$\hat{\tau}_{22} = \begin{pmatrix} T_{44} & 0 \\ T_{34} & 0 \end{pmatrix} . \qquad (A.2d)$$

Here, the T_{ij} are elements of Budden's T matrix [Eq. (1)]. Substituting Eqs. (A.2) into Eq. (A.1), we have the forms for the admittance in the general case:

$$\frac{i}{k} \frac{d}{dz} A_{11} = T_{41} - T_{14}A_{11}^2 + A_{11}(T_{44} - T_{11}) + A_{12}A_{21} ,$$

$$\frac{i}{k} \frac{d}{dz} A_{12} = -T_{42} + A_{12}(-T_{14}A_{11} + A_{22} + T_{44}) + T_{12}A_{11} ,$$

$$\frac{i}{k} \frac{d}{dz} A_{21} = T_{31} + A_{21}(-T_{14}A_{11} + A_{22} - T_{11}) + T_{34}A_{11} ,$$

$$\frac{i}{k} \frac{d}{dz} A_{22} = -T_{32} + A_{22}^2 - T_{14}A_{12}A_{21} + T_{12}A_{21} + T_{34}A_{12} .$$

INITIAL VALUES FOR ADMITTANCE

We will use our normal coordinate system. Assume a sharply bounded ionosphere with a wave incident from below, and assume we know q (the solution of the Booker quartic in the ionosphere). Then the Maxwell equations become

$$qE_y = -H_x , \qquad -qE_x + SE_z = -H_y , \qquad -SE_y = -H_z ,$$

and

$$qH_y = [(\hat{I} + \hat{M})\vec{E}]_x \ , \qquad -qH_x + SH_z = [(\hat{I} + \hat{M})\vec{E}]_y \ , \qquad -SH_y = [(\hat{I} + \hat{M})\vec{E}]_z \ .$$

By combining these equations, we obtain

$$\begin{pmatrix} -q^2 & 0 & qS \\ 0 & -q^2 - S^2 & 0 \\ qS & 0 & -S^2 \end{pmatrix} \begin{pmatrix} E_x \\ E_y \\ E_z \end{pmatrix} = -(\hat{I} + \hat{M})\vec{E} \qquad (A.3)$$

or, with obvious notation,

$$(\hat{L} + \hat{I} + \hat{M})\vec{E} = 0 \ .$$

Then, for a nontrivial solution to exist,

$$|\hat{L} + \hat{I} + \hat{M}| = 0 \ .$$

This leads to Booker's quartic, which we solve using the method of Sheddy [1968].

Let q be a solution of Booker's quartic and define

$$\hat{D}(q) = \hat{L}(q) + \hat{I} + \hat{M} \ .$$

Now expanding Eq. (A.3), we get

$$D_{11}E_x + D_{12}E_y + D_{13}E_z = 0 \ , \qquad (A.4a)$$

$$D_{21}E_x + D_{22}E_y + D_{23}E_z = 0 \ , \qquad (A.4b)$$

$$D_{31}E_x + D_{32}E_y + D_{33}E_z = 0 \ . \qquad (A.4c)$$

To find expressions for E_x and E_z in terms of E_y, we use Eqs. (A.4a) and (A.4c). Then

$$E_x = -\frac{D_{33}D_{12} - D_{13}D_{32}}{D_{33}D_{11} - D_{13}D_{31}} E_y \equiv PE_y , \qquad (A.5a)$$

$$E_z = \frac{D_{31}D_{12} - D_{11}D_{32}}{D_{33}D_{11} - D_{13}D_{31}} E_y \equiv QE_y . \qquad (A.5b)$$

Also,[*]

$$H_x = -qE_y , \qquad (A.6a)$$

$$H_y = qE_x - SE_z = (qP - SQ)E_y \equiv TE_y . \qquad (A.6b)$$

The definition of admittance [Budden, 1961] is

$$\hat{A} = \begin{pmatrix} H_y^{(1)} & H_y^{(2)} \\ H_y^{(1)} & H_x^{(2)} \end{pmatrix} \begin{pmatrix} E_x^{(1)} & E_x^{(2)} \\ E_y^{(1)} & E_y^{(2)} \end{pmatrix}^{-1} , \qquad (A.7)$$

where the superscripted (1) and (2) denote one solution of the Booker quartic. There are, in general, four solutions: two represent upgoing waves (Imq < 0) and two represent downgoing waves (Imq > 0). At this point, only upgoing waves are present.

If we let $E_y^{(2)} = aE_y^{(1)}$, then we can solve Eq. (A.7). Substituting Eqs. (A.5) and (A.6) into Eq. (A.7) gives

---

[*]Here we adopt the notation of Sheddy [1968].

$$
\hat{A} = \begin{pmatrix} T_1 & T_2 a \\ -q_1 & -q_2 a \end{pmatrix} \begin{pmatrix} P_1 & P_2 a \\ 1 & a \end{pmatrix}^{-1}
$$

$$
= \begin{pmatrix} T_1 - T_2 & T_2 P_1 - T_1 P_2 \\ q_2 - q_1 & q_1 P_2 - q_2 P_1 \end{pmatrix} \frac{1}{P_1 - P_2} \ . \tag{A.8}
$$

Equation (A.8) works only in the anisotropic case. In the iso-tropic case,

$$
M_{ij} = M \delta_{ij} \ ,
$$

where

$$
M = n^2 - 1 \ .
$$

The Maxwell equations separate into two sets: the transverse electric, i.e.,

$$
qE_y = -H_x \ , \qquad -SE_y = -H_z \ , \qquad -qH_x + SH_z = n^2 E_y \ ;
$$

and the transverse magnetic, i.e.,

$$
-qE_x + SE_z = -H_y \ , \qquad qH_y = n^2 E_x \ , \qquad -SH_y = n^2 E_z \ .
$$

Both sets lead to $q^2 = n^2 - S^2$. We can take

$$
E_y^{(1)} = H_x^{(1)} = 0 \quad \text{and} \quad E_x^{(2)} = H_y^{(2)} = 0 \ .
$$

Therefore,

$$\hat{A} = \begin{pmatrix} H_y^{(1)} & 0 \\ \\ 0 & H_x^{(2)} \end{pmatrix} \begin{pmatrix} E_x^{(1)} & 0 \\ \\ 0 & D_y^{(2)} \end{pmatrix}^{-1}$$

$$= \begin{pmatrix} \dfrac{H_y^{(1)}}{E_x^{(1)}} & 0 \\ \\ 0 & \dfrac{H_x^{(2)}}{E_y^{(2)}} \end{pmatrix} = \begin{pmatrix} \dfrac{n^2}{q} & 0 \\ \\ 0 & -q \end{pmatrix} .$$

In free space, when $n^2 \cong 1$,

$$q^2 = n^2 - S^2 = 1 - S^2 = C^2 \quad \text{and so} \quad \hat{A} = \begin{pmatrix} \dfrac{1}{C} & 0 \\ \\ 0 & -C \end{pmatrix} .$$

Appendix B

COLLISION FREQUENCY

This appendix presents the electron/neutral ion collision frequency as a function of height. We take the values for collision frequency from the tables given by Pappert and Moler [1974]. We use nighttime collision frequency data for all cases because daytime and nighttime frequencies are the same up to 160 km, and we do not expect to need frequencies above 160 km for daytime cases.

Table B.1

ELECTRON/NEUTRAL ION COLLISION
FREQUENCY VERSUS ALTITUDE

Altitude (km)	Collision Frequency (sec^{-1})
250.00	1.05E 02
225.00	3.50E 01
220.00	3.00E 01
210.00	3.30E 01
200.00	4.50E 01
150.00	1.60E 03
120.00	1.00E 04
100.00	3.90E 04
0.0	4.30E 11

Appendix C

CALCULATION OF UPGOING FIELDS

This appendix derives the equations for the upgoing fields. Since nearly all quantities here are matrices, we drop the caret matrix notation. Budden [1961] defines the up- and downgoing fields as, respectively,

$$U = \frac{1}{2} (I_1 E + I_2 H) , \qquad (C.1)$$

$$D = \frac{1}{2} (I_3 E + I_4 H) , \qquad (C.2)$$

where

$$I_1 = \begin{pmatrix} \frac{1}{C} & 0 \\ 0 & 1 \end{pmatrix} , \qquad I_2 = \begin{pmatrix} 1 & 0 \\ 0 & -\frac{1}{C} \end{pmatrix} ,$$

$$\qquad (C.3)$$

$$I_3 = \begin{pmatrix} -\frac{1}{C} & 0 \\ 0 & 1 \end{pmatrix} , \qquad I_4 = \begin{pmatrix} 1 & 0 \\ 0 & \frac{1}{C} \end{pmatrix} .$$

We also know that $H = AE$ and $D = RU$.

Combining Eqs. (C.1) and (C.2), we see that

$$E = \left(I_1^{-1} U + I_3^{-1} D \right) + \frac{1}{2} \left(I_1^{-1} I_2 + I_3^{-1} I_4 \right) H .$$

But it is easy to show that

$$I_1^{-1} I_2 = -I_3^{-1} I_4 .$$

So

$$E = I_1^{-1}U + I_3^{-1}D . \qquad (C.4)$$

Now using Eqs. (C.1) and (C.4) and the fact that

$$I_2^{-1}I_1I_3^{-1} = I_4^{-1} ,$$

we obtain

$$H = I_2^{-1}U + I_4^{-1}D . \qquad (C.5)$$

Budden gives the derivatives of E and H as

$$\frac{i}{k} E' = -\tau_{11}E - \tau_{12}H , \qquad (C.6)$$

$$\frac{i}{k} H' = \tau_{21}E + \tau_{22}H , \qquad (C.7)$$

where τ is as defined by Eqs. (A.2). If we differentiate Eq. (C.1), we get

$$\frac{i}{k} U' = \frac{1}{2} (I_1E' + I_2H') . \qquad (C.8)$$

Putting Eqs. (C.6) and (C.7) into Eq. (C.8) and then using Eqs. (C.4) and (C.5), we have

$$\frac{i}{k} U' = \frac{1}{2} (S_1U + S_2D) , \qquad (C.9)$$

where

$$S_1 = -I_1 \left(\tau_{11} I_1^{-1} + \tau_{12} I_2^{-1} \right) + I_2 \left(\tau_{21} I_1^{-1} + \tau_{22} I_2^{-1} \right) \ ,$$

$$S_2 = -I_1 \left(\tau_{11} I_3^{-1} + \tau_{12} I_4^{-1} \right) + I_2 \left(\tau_{21} I_3^{-1} + \tau_{22} I_4^{-1 } \right) \ .$$

After some matrix manipulation, we obtain

$$S_1 = \begin{pmatrix} T_{11} + \dfrac{T_{14}}{C} + CT_{41} + T_{44} & -\dfrac{T_{12}}{C} - T_{42} \\[2em] -T_{31} - \dfrac{T_{34}}{C} & C + T_{32} \end{pmatrix} \qquad (C.10)$$

and

$$S_2 = \begin{pmatrix} -T_{11} + \dfrac{T_{14}}{C} - CT_{41} + T_{44} & -\dfrac{T_{12}}{C} - T_{42} \\[2em] T_{31} - \dfrac{T_{34}}{C} & -C + T_{32} \end{pmatrix} . \qquad (C.11)$$

The matrices S_1 and S_2 are the same as $S^{(11)}$ and $S^{(12)}$, defined in Sec. II.

Entering $D = RU$ into Eq. (C.9) yields

$$\frac{i}{k} U' = \frac{1}{2} (S_1 + S_2 R) U \ . \qquad (C.12)$$

It is useful to know the fields in free space. Section II shows that

$$S_1 = 2CI \quad \text{and} \quad S_2 = 0 \ .$$

Therefore, Eq. (C.12) becomes

$$U' = -ikCU ,$$

which gives

$$U_{ij}(z) = U_{ij}(0) \, e^{-ikCz} . \qquad (C.13)$$

REFERENCES

Budden, K. G., *Radio Waves in the Ionosphere*, Cambridge University Press, London, 1961.

Field, E. C., R. E. Warren, and C. R. Warber, "Calculation of Ionospheric Conductivity Profiles by Inverting VLF/LF Reflection Data: I. Isotropic Propagation," *Radio Sci.*, Vol. 18, No. 3, May–June 1983, pp. 452-460.

Pappert, R. A., and W. F. Moler, "Propagation Theory and Calculations at Lower ELF," *IEEE Trans. Comm.*, Vol. COM-22, No. 4, April 1974, pp. 438-451.

Reagan, J. B., et al., "Modeling of the Ambient and Disturbed Ionospheric Media Pertinent to ELF/VLF Propagation," *AGARD Conference Proceedings 305*, 1982, pp. 33-1 through 33-10.

Sheddy, C. H., "A General Analytic Solution for Reflection from a Sharply Bounded Anisotropic Ionosphere," *Radio Sci.*, Vol. 3, No. 8, August 1968, pp. 792-795.

Warren, R. E., E. C. Field, and C. R. Warber, *Calculation of Ionospheric Conductivity Profiles by Inverting VLF/LF Reflection Data: I. Isotropic Propagation*, Rome Air Development Center, Griffiss Air Force Base, New York, RADC-TR-81-286, October 1981 (also published as PSR Report 1114, May 1981).

MISSION
of
Rome Air Development Center

RADC plans and executes research, development, test and selected acquisition programs in support of Command, Control Communications and Intelligence (C^3I) activities. Technical and engineering support within areas of technical competence is provided to ESD Program Offices (POs) and other ESD elements. The principal technical mission areas are communications, electromagnetic guidance and control, surveillance of ground and aerospace objects, intelligence data collection and handling, information system technology, solid state sciences, electromagnetics and electronic reliability, maintainability and compatibility.

END

FILMED

3-85

DTIC